Robotica (2009) volume 27, pp. 841–852. © Cambridge University Press 2008
doi:10.1017/S0263574708005225

Optimal design and implementation of an energy-efficient biped walking in semi-active manner

Ting-Ying Wu and T.-J. Yeh*

Department of Power Mechanical Engineering, National Tsing Hua University, Hsinchu, Taiwan, R.O.C.

(Received in Final Form: October 28, 2008. First published online: December 2, 2008)

SUMMARY

In this paper, a biped that combines the merits of both powered and passive bipeds is proposed. The semi-activeness of the biped is due to the fact that during most of a walking cycle, only half of the joints are actuated to follow specific trajectories, and the other half of joints remain unactuated but have passive springs connected between adjacent links. It is expected that by having unactuated joints, the biped can preserve the power-saving feature of the passive biped, and by having actuated joints under active control, the biped can also achieve the stability and performance of the powered biped. To devise a systematic design methodology for the biped, its dynamics as well as the walking constraints are carefully studied. Furthermore, an optimization procedure is also proposed to compute the optimal trajectories for the actuated joints and spring constants, which can lead to minimum energy consumption. The feasibility of the proposed biped, including the system design and the control strategy, is verified by hardware implementation. Experiments indicate that the biped walking in the semi-active manner consumes 80% less the electrical power than the fully powered biped that performs the same gait and is more energy-efficient than several state-of-the-art bipeds.

KEYWORDS: Semi-activeness; Passive biped; Powered biped; Nonlinear optimization.

1. Introduction

Depending on whether power sources are needed, bipedal walkers can be divided into two categories: powered bipeds and passive bipeds. Powered bipeds rely heavily on external power and active control to achieve the walking motion. In these systems, there is usually an actuator located at each joint. The actuators are servo-controlled to make the joints follow a set of reference trajectories that are planned in advance based on the desired walking pattern and stability considerations.[1] Despite the fact that powered bipeds can produce dexterous and human-like motions, these systems often consume excessive power. Take the humanoid robot P3[2] for example, its power consumption during walking is about 2 kW, which is approximately 20 times the power consumption of a human of the same size.

* Corresponding author. email: d927706@oz.nthu.edu.tw; tyeh@pme.nthu.edu.tw

On the other hand, the passive bipeds, as proposed first by McGeer,[3] demand neither external power nor active control. Their motion is solely the result of interaction between gravity and the passive dynamics of the biped itself. Although passive bipeds consume zero power, their stability and reliability are usually the main source of concern. For instance, the passive biped developed by Collins, Wisse and Ruina[4] still has a failure rate of more than 20%; moreover, the walking is limited to going down a slope. It should be noted that the walking of the bipeds presented by Collins et al.[5] is also based on passive dynamics. However, with active power sources incorporated to selected joints to substitute the gravitational power, the bipeds can walk on a level ground.

In this research, we intend to integrate the merits of both the powered and passive bipeds by developing a biped that walks in a semi-active manner. The developed biped, similar to those discussed in Collins et al.,[5] falls in the category of under-actuated bipeds, in which only part of the joints are actuated and the rest remain unactuated. The design and control of such a biped is particularly addressed by optimizing the trajectories of the actuated joints and the incorporated joint springs so as to minimize the input energy. In the literature, there is research addressing the design and control issues for either the fully actuated or underactuated bipeds from similar viewpoints. For example, Bessonnet, Seguin, and Sardain[6] derived an optimal gait for a fully actuated, seven-link planar biped to minimize the input energy. In Sangwan and Agrawal,[7] differential flatness was used to control an underactuated, 2 degrees-of-freedom (DOF) linkage. In order to have the linkage produce a leg-like swing motion, numerical optimization was performed to compute the flat output trajectories and system parameters, including the knee joint spring and its equilibrium position. Ono and Liu[8] numerically investigated the optimal and sub-optimal joint trajectories for a simple 3-link biped respectively, under full-actuation and under-actuation. Ono, Furuichi, and Takahashi[9] also experimentally constructed 3-DOF planar bipeds that can perform self-excited walking by actuating a motor at the hip joint and using active lock mechanisms at both knee joints. Westervelt, Buche and Grizzle[10] proposed a framework for the design of controllers that induce stable walking in underactuated, planar bipeds. In their bipeds, the underactuation comes from the point-foot configuration during the single-support phase. The controllers therein make the joints track posture-dependent trajectories that are computed based on minimization of actuator torques and invariance of hybrid zero dynamics

https://doi.org/10.1017/S0263574708005225 Published online by Cambridge University Press

under the foot impact. In Westervelt et al.,[11] the authors also applied a similar design methodology to a seven-link, planar bipedal model with non-trivial feet and under-actuated phase occurring when the stance heel rises from the ground and the stance foot rotates about the stance toe.

The basic design and control philosophy of the proposed biped can be best understood by examining the principle of energy conservation for each walking cycle. Assuming that the biped performs stable and periodic walking on a level ground, then we have:

$$0 = W_+ - W_- - \Delta E_{\text{lost}}, \tag{1}$$

where W_+ and W_- are respectively the positive work and the negative work done by the actuators, and ΔE_{lost} denotes the energy loss due to friction and foot-ground impact. The right side of the equation equals zero because it corresponds to the change of internal energy in one cycle and should vanish by the periodicity assumption. It should be noted that most actuators used in bipeds are non-regenerative, so negative work is not recoverable. This indicates that positive work alone contributes to the energy consumption of the biped. Since (1) equivalently gives $W_+ = \Delta E_{\text{lost}} + W_-$, it is clear that minimizing the energy consumption amounts to keep the energy loss and non-recoverable negative work to minimum.

Intuitively, one can reduce the energy consumption by incorporating mechanical springs to joints of the biped. This is because springs are a natural means of energy storage and the negative work absorbed by them is recoverable. Besides, the torques resulting from spring deformations can support the weight of the biped, so the actuation torques counteracting the gravity are relieved. Finally, the biped, which is originally open and unstable, can have its instability reduced if there are springs attached to the joints. Another intuitive way to reduce the energy consumption is activating only part of the actuators and leaving the others unactuated. By doing so, not only is the total number of actuators performing the work reduced, but also the passive dynamics of the biped is less interfered with so that it can be better exploited for energy efficiency purposes. Following this line of thought, in the proposed biped, at each joint there is a torsional spring in parallel with the actuator and the biped walks based on a semi-active control strategy, that is, only the actuators in one leg are in actuation and the actuators in the other leg are in relaxation.

The rest of the paper is devoted to optimal design and implementation of this biped walking in a semi-active manner and is organized as follows. In Section 2, the gait for semi-active walking is described and the associated dynamics are analyzed. Section 3 investigates the constraints to achieve human-like, continuous, stable walking. In Section 4, an optimization procedure is proposed to compute the optimal trajectories for the actuated joints and spring constants, which can lead to minimum energy consumption. Numerical results associated with the optimization are presented in Section 5. In Section 6, a prototype is constructed based on the optimization results and its performance is verified experimentally. Finally, the conclusions are given in Section 7.

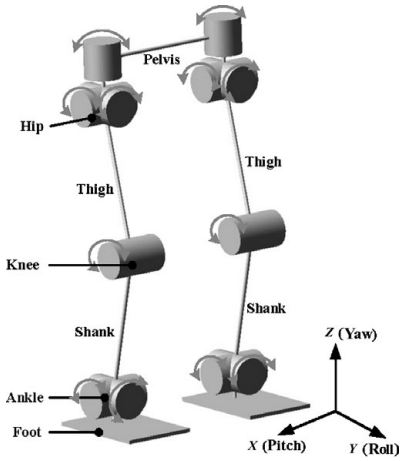


Fig. 1. The 12-DOF model of the semi-active biped.

2. Dynamics for the Biped Walking in a Semi-Active Manner

The biped considered has 12-DOF and its configuration is depicted in Fig. 1. According to this figure, each leg of the biped contains six revolute joints with two at the ankle, one at the knee, and three at the hip. At each revolute joint, there is a parallel combination of a rotary actuator and a torsional spring. Therefore, if the actuator is not powered, the corresponding joint is completely passive and the joint motion is only dictated by the spring. In the following discussion, the leg in actuation will be referred to as the active leg, and the leg in relaxation will be referred to as the passive leg.

In Fig. 2, the stick diagrams of the biped in one semi-active walking step are shown respectively in the sagittal and the frontal views. In the diagrams, the active leg is depicted by bold line segments and the passive leg by thin line segments. One walking step consists of five consecutive postures (1–5): at posture 1, both feet of the biped are in contact with ground. However, the rear (right, passive) foot is about to be lifted off the ground so that the biped at this posture is completely supported by the left (front, active) leg. At posture 2, the right foot has already been lifted and is swinging towards the front. At posture 3, the right foot just lands on the ground and becomes the front foot. At posture 4, the projection of the pelvis is around the middle of the two feet and the front (right) leg becomes the active leg at this instant. Finally, at posture 5, the biped resumes the same posture as posture 1 except that the legs are exchanged. Let t_i denote the time instant when the ith posture occurs. Then from t_1^+ to t_3^-, the biped is in single support phase (SSP) and from t_3 to t_5 the biped is in double support phase (DSP). Moreover, from t_1 to t_4^- the left leg is active and the right leg is passive; and from t_4 to t_5 the right leg is active and the left leg is passive.

The models for defining crucial variables for dynamic analyses in the sagittal and frontal planes are shown in Fig. 3. In these models, the symbols $\theta_{i,p}$ and $\theta_{i,r}$ are the ith joint angles, respectively in the pitch and roll directions. For simplification, it is assumed that the hip's yaw and roll angles are properly regulated by the controllers so that the pelvis link is always perpendicular to the sagittal plane and parallel

https://doi.org/10.1017/S0263574708005225 Published online by Cambridge University Press

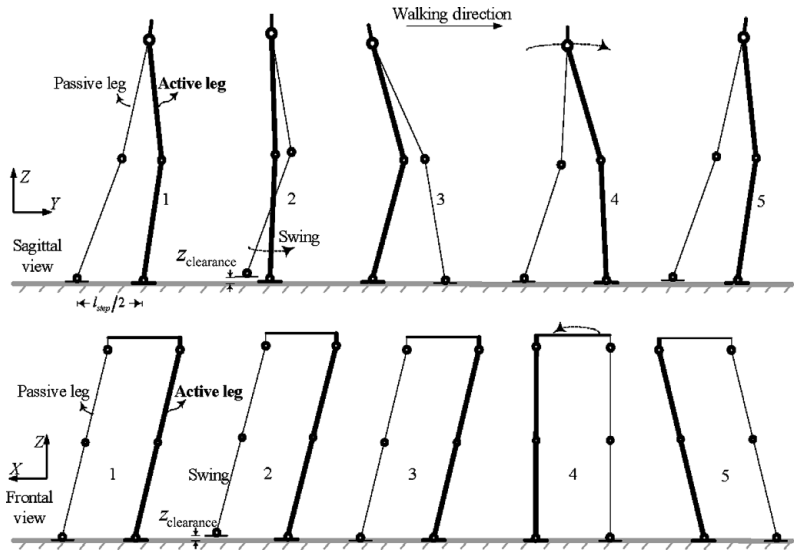


Fig. 2. The schematic figures of the semi-active locomotion in a walking step.

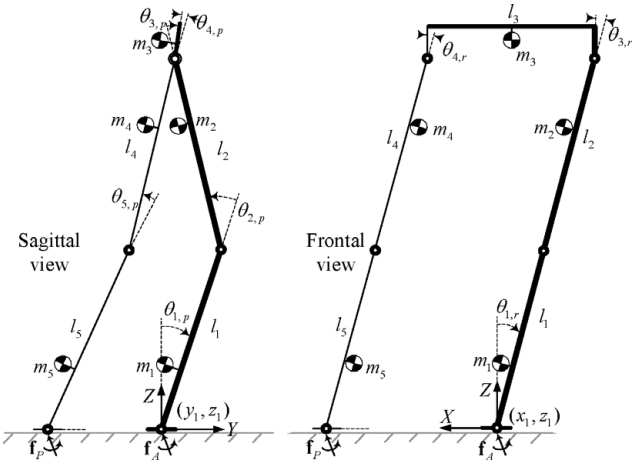


Fig. 3. Definitions of crucial variables for dynamic analysis.

to the frontal plane. With this assumption, the dynamics in the sagittal and frontal planes become decoupled and the associated dynamics therefore can be derived independently. When the foot of the active leg is also assumed to be fixed to the ground, the equation of motion in either plane can be formulated in the following form:

$$\mathbf{M}(\boldsymbol{\theta})\cdot\ddot{\boldsymbol{\theta}} + \mathbf{C}(\boldsymbol{\theta}, \dot{\boldsymbol{\theta}})\cdot\dot{\boldsymbol{\theta}} + \mathbf{g}(\boldsymbol{\theta}) + \mathbf{d}(\dot{\boldsymbol{\theta}}) + \mathbf{K}\cdot(\boldsymbol{\theta} - \bar{\boldsymbol{\theta}}) = \boldsymbol{\tau} + \mathbf{J}(\boldsymbol{\theta})^T\cdot\mathbf{f}_P. \quad (2)$$

In this equation, $\boldsymbol{\theta}$ equals $[\theta_{1,p}\ \theta_{2,p}\ \theta_{3,p}\ \theta_{4,p}\ \theta_{5,p}]^T$ for the sagittal dynamics and equals $[\theta_{1,r}\ \theta_{3,r}\ \theta_{4,r}]^T$ for the frontal dynamics, $\mathbf{M}$ is the inertia matrix, $\mathbf{C}$ is a matrix related to the Coriolis and centrifugal effects, $\mathbf{g}$ is the gravitational torque vector, $\mathbf{d}$ is the torque vector associated joint damping, $\mathbf{K}\cdot(\boldsymbol{\theta} - \bar{\boldsymbol{\theta}})$ is the torque vector generated by the passive springs at the joints that $\mathbf{K} = \text{diag}[k_{1,p}\ k_{2,p}\ k_{3,p}\ k_{4,p}\ k_{5,p}]$ for the sagittal dynamics, $\mathbf{K} = \text{diag}[k_{1,r}\ k_{3,r}\ k_{4,r}]$[†] for the frontal dynamics and $\bar{\boldsymbol{\theta}}$ is the vector corresponding to springs' relaxed angles, $\boldsymbol{\tau}$ is a vector corresponding to actuation torques at the joints and due to the semi-active nature of the actuation, $\boldsymbol{\tau} = [\tau_{1,p}\ \tau_{2,p}\ \tau_{3,p}\ 0\ 0]^T$ for the sagittal dynamics and $\boldsymbol{\tau} = [\tau_{1,r}\ \tau_{3,r}\ 0]^T$ for the frontal dynamics and finally $\mathbf{f}_P$ is the vector that represents the interaction force/moment between the passive foot and the ground, with $\mathbf{J}(\boldsymbol{\theta})$ being the associated Jacobian matrix. It should be noted that in the formulation, to further simplify the problem, the size and the weight of the foot are assumed to be negligible, so the influence of the spring toque $k_{6,*}\cdot(\theta_{6,*} - \bar{\theta}_{6,*})$ can be lumped into the interaction force/moment vector $\mathbf{f}_P$.

By the special structure in $\boldsymbol{\tau}$, (2) can be partitioned as follows:

$$\mathbf{M}_a(\boldsymbol{\theta})\cdot\ddot{\boldsymbol{\theta}} + \mathbf{C}_a(\boldsymbol{\theta}, \dot{\boldsymbol{\theta}})\cdot\dot{\boldsymbol{\theta}} + \mathbf{g}_a(\boldsymbol{\theta}) + \mathbf{K}_a\cdot(\boldsymbol{\theta}_a - \bar{\boldsymbol{\theta}}_a) + \mathbf{d}_a(\dot{\boldsymbol{\theta}}_a) = \boldsymbol{\tau}_a + \mathbf{J}_a(\boldsymbol{\theta})^T\cdot\mathbf{f}_P, \quad (3)$$

$$\mathbf{M}_u(\boldsymbol{\theta})\cdot\ddot{\boldsymbol{\theta}} + \mathbf{C}_u(\boldsymbol{\theta}, \dot{\boldsymbol{\theta}})\cdot\dot{\boldsymbol{\theta}} + \mathbf{g}_u(\boldsymbol{\theta}) + \mathbf{K}_u\cdot(\boldsymbol{\theta}_u - \bar{\boldsymbol{\theta}}_u) + \mathbf{d}_u(\dot{\boldsymbol{\theta}}_u) = \mathbf{0} + \mathbf{J}_u(\boldsymbol{\theta})^T\cdot\mathbf{f}_P. \quad (4)$$

In the two equations, the subscripts a and u respectively denote the actuated and unactuated part of the vector/matrix. For example, $\boldsymbol{\theta}_a = [\theta_{1,p}\ \theta_{2,p}\ \theta_{3,p}]^T$, $[\theta_{4,p}\ \theta_{5,p}]^T$ and $\boldsymbol{\tau}_a = [\tau_{1,p}\ \tau_{2,p}\ \tau_{3,p}]^T$ for the sagittal dynamics; $\boldsymbol{\theta}_a = [\theta_{1,r}\ \theta_{3,r}]^T$, $\boldsymbol{\theta}_u = \theta_{4,r}$ and $\boldsymbol{\tau}_a = [\tau_{1,r}\ \tau_{3,r}]^T$ for the frontal dynamics.

During the SSP, if the passive/unactuated leg swings without foot-ground contact, then $\mathbf{f}_P = \mathbf{0}$. Therefore, given $\mathbf{K}_u$ and $\boldsymbol{\theta}_a(t)$,[‡] the Runge–Kutta method can be applied to integrate (4) to numerically solve for $\boldsymbol{\theta}_u(t)$. Here an operator $\boldsymbol{\Gamma}_{SSP}$ is used to denote the functional dependency between $\boldsymbol{\theta}_u(t)$ and $\boldsymbol{\theta}_a(t)$, $\mathbf{K}_u$ or

$$\boldsymbol{\theta}_u(t) = \boldsymbol{\Gamma}_{\text{SSP}}(\boldsymbol{\theta}_a(t), \mathbf{K}_u). \quad (5)$$

[†] The symbol $k_{*,*}$ represents the spring constant. Its subscripts denote which joint the spring is attached to.

[‡] In analysing the dynamic equations, it is assumed that the geometry, mass/inertia properties, the damping properties as well as the relaxed spring angles have already been determined.

https://doi.org/10.1017/S0263574708005225 Published online by Cambridge University Press

On the other hand, during the DSP, both feet of the biped are in contact with the ground so that the two legs and the ground form a closed-loop chain. By kinematic analysis, $\boldsymbol{\theta}_u(t)$ can be derived as an algebraic function of $\boldsymbol{\theta}_a(t)$. Denoting such an algebraic function by $\boldsymbol{\Gamma}_{\text{DSP}}$, then

$$\boldsymbol{\theta}_u(t) = \boldsymbol{\Gamma}_{\text{DSP}}(\boldsymbol{\theta}_a(t)). \tag{6}$$

Substituting this algebraic relation into (4) and assuming that $\mathbf{J}_u(\boldsymbol{\theta})$ is non-singular, one can directly solve for $\mathbf{f}_P$. Another operator $\boldsymbol{\Gamma}_{\mathbf{f}_P}$ is used to denote the functional dependency between $\mathbf{f}_P$ and $\boldsymbol{\theta}_a(t)$, $\mathbf{K}_u$ or

$$\mathbf{f}_P = \boldsymbol{\Gamma}_{\mathbf{f}_P}(\boldsymbol{\theta}_a(t), \mathbf{K}_u). \tag{7}$$

Once $\boldsymbol{\theta}_a(t)$ $\boldsymbol{\theta}_u(t)$, and $\mathbf{f}_P$ are known and $\mathbf{K}_a$ are given, one can compute the actuation torque $\boldsymbol{\tau}_a$ using (3). This, together with (5) (in SSP) or (6) and (7) (in DSP), implies that $\boldsymbol{\tau}_a$ is dictated by $\boldsymbol{\theta}_a(t)$ and $\mathbf{K}$, or $\boldsymbol{\tau}_a$ can be succinctly written as

$$\boldsymbol{\tau}_a = \boldsymbol{\Gamma}_{\boldsymbol{\tau}_a}(\boldsymbol{\theta}_a(t), \mathbf{K}), \tag{8}$$

where $\boldsymbol{\Gamma}_{\boldsymbol{\tau}_a}$ is the operator denoting the functional dependency. Furthermore, by treating the biped as a system of particles (with the ith link modeled as a point mass m_i), assuming the knowledge of $\mathbf{f}_P(=\mathbf{0}$ for SSP, $=$ (7) for DSP), and $\boldsymbol{\theta}_a(t)$, $\boldsymbol{\theta}_u(t)$ (consequently the acceleration of each point mass), and then applying Newton's equations of motion to the whole biped, the interaction force/moment vector between the active foot and the ground can be solved. Again by (5) (in SSP) or (6) and (7) (in DSP), $\boldsymbol{\theta}_a(t)$ and $\mathbf{K}_u$ alone determine $\mathbf{f}_A$. Denoting the functional dependency by $\boldsymbol{\Gamma}_{\mathbf{f}_A}$, we have

$$\mathbf{f}_A = \boldsymbol{\Gamma}_{\mathbf{f}_A}(\boldsymbol{\theta}_a(t), \mathbf{K}_u). \tag{9}$$

3. Constraints for Achieving Stable, Periodical, Semi-active Walking

The above dynamic analysis shows that whenever the trajectories of the active leg ($\boldsymbol{\theta}_a(t)$) and the spring constants ($\mathbf{K}$) are given, the trajectories of the passive leg ($\boldsymbol{\theta}_u(t)$), the actuation torques ($\boldsymbol{\tau}_a$), and the foot-ground contact forces/moments ($\mathbf{f}_A$,$\mathbf{f}_P$) can be computed accordingly. One main purpose of the paper is to devise an optimal solution for $\boldsymbol{\theta}_a(t)$ and $\mathbf{K}$ so that the biped can perform stable, periodical, semi-active walking in an energy-efficient manner. To do so, constraints on the joint trajectories are investigated. The constraints will be incorporated into the numerical procedure subsequently to determine the optimal joint trajectories and spring constants.

Basically, there are four types of constraints. These are explained below:

(1) Constraints for continuity: From the discussion in Fig. 2, transitions between SSP and DSP occur at postures 1, 3, 5 and control authority transfers from the left leg to the right leg at posture 4. At these four postures, the biped experiences drastic dynamic change. Regardless of the dynamic change, both the joint angles and the angular velocities should be continuous at the associated time instants. In other words,

$$\boldsymbol{\theta}(t_i^-) = \boldsymbol{\theta}(t_i) = \boldsymbol{\theta}(t_i^+)\text{ , for } i = 1, 3, 4 \text{ and } 5. \tag{10}$$

and

$$\dot{\boldsymbol{\theta}}(t_i^-) = \dot{\boldsymbol{\theta}}(t_i) = \dot{\boldsymbol{\theta}}(t_i^+)\text{ , for } i = 1, 3, 4 \text{ and } 5. \tag{11}$$

Note that at posture 4, the active leg of the biped switches from the rear (left) to the front (right) leg. Therefore, by the definitions of variables in Fig. 3, the index for respective components of $\boldsymbol{\theta}$ should also switch accordingly at $t = t_4$.

(2) Constraints for quasi-static postures: In order for the biped to walk similar to a human being, the joint angles at postures 1, 3 and 5 are specified appropriately. Moreover, because the biped experiences dynamic change at these postures, to reduce the impact of the dynamic changes towards motion smoothness, the biped is also assumed to be in quasi-static state at postures 1, 3 and 5. The corresponding constraints are written explicitly as:

$$\boldsymbol{\theta}(t_j) = \boldsymbol{\theta}_d^j \text{ and } \dot{\boldsymbol{\theta}}(t_j) = \mathbf{0}, \quad \text{for } j = 1, 3 \text{ and } 5, \tag{12}$$

where $\boldsymbol{\theta}_d^j$ is the specified joint angle vector at posture j. Notice that the choice of $\boldsymbol{\theta}_d^j$'s is not arbitrary but needs to meet three conditions. First of all, the actuated and unactuated parts in $\boldsymbol{\theta}_d^j$'s should satisfy the algebraic equation in (6). The second condition is that $\boldsymbol{\theta}_d^1 = \boldsymbol{\theta}_d^5$ so as to establish the walking periodicity. Finally, the three $\boldsymbol{\theta}_d^j$'s should lead to a consistent step length l_{step}. With l_{step} and the time instants for the transiting postures assigned, the average walking speed is given by $\frac{l_{\text{step}}}{2(t_5 - t_1)}$.

(3) Constraints for foot-ground clearance: During the entire SSP it is crucial that the passive (swing) foot should maintain a certain clearance from the ground to avoid the foot-ground interference. Such a constraint is given by

$$z_{\text{clearance}}(\boldsymbol{\theta}(t)) > 0, \quad \text{for } t \in [t_1^+ , t_3^-], \tag{13}$$

where $z_{\text{clearance}}$ denotes the clearance between the passive foot and the ground, and its functional dependency on $\boldsymbol{\theta}(t)$ can be easily derived using the bipedal geometry. By the configuration and the quasi-static property of posture 3, $z_{\text{clearance}}|_{t=t_3} = 0$ and the landing velocity of the swing foot also vanishes. Therefore, foot-ground impact is eliminated in this case.

(4) Constraints for stability: Two more constraints need to be satisfied in order for the biped to walk in a stable manner. One is that sliding should not occur for the foot (feet) in contact with the ground. Such a constraint is relevant to $\mathbf{f}_A$ and $\mathbf{f}_P$. In the sagittal (frontal) dynamics, both $\mathbf{f}_A$ and $\mathbf{f}_P$ have three components: A force in y (x) direction, a force in z direction, and a moment in x (y) direction. The y (x)-force, which also acts in the tangential direction, is denoted by $(\mathbf{f}_{(\cdot)})_t$. The z-force, which also acts in the normal direction, is denoted by $(\mathbf{f}_{(\cdot)})_n$. Finally, the moment component, which is in respect to the ankle joint of the foot in discussion (i.e. passive foot for $\mathbf{f}_P$ and active

https://doi.org/10.1017/S0263574708005225 Published online by Cambridge University Press

foot for $\mathbf{f}_A$), is denoted by $(\mathbf{f}_{(\cdot)})_m$. To prevent the foot from sliding, we should have

$$|(\mathbf{f}_A)_t| \le \mu_s(\mathbf{f}_A)_n \text{ and } |(\mathbf{f}_P)_t| \le \mu_s(\mathbf{f}_P)_n, \qquad (14)$$

where μ_s is the coefficient of static friction. Equation (14) implicitly constrains $(\mathbf{f}_{(\cdot)})_n$'s to be non-negative, which comes from the uni-directionality of the ground reaction. Furthermore, in the case of SSP, $\mathbf{f}_P = 0$, so the passive part of (14) is automatically satisfied.

The other stability constraint is that during walking the biped should be in dynamic equilibrium so that it does not fall down. This constraint is equivalent to limiting the total zero moment point (ZMP) associated $\mathbf{f}_A$ and $\mathbf{f}_P$ to be strictly inside the support polygon spanned by the foot (feet) contacting the ground.[12] The ZMP can be easily derived as a function of the components in $\mathbf{f}_A$ and $\mathbf{f}_P$. Take the sagittal dynamics for example, when the passive (active) foot is in front of the active (passive) foot, the ZMP is located at $\frac{(\mathbf{f}_A)_m+(\mathbf{f}_P)_m+(\mathbf{f}_P)_n\cdot l_{\text{step}}}{(\mathbf{f}_A)_n+(\mathbf{f}_P)_n}$ ($\frac{(\mathbf{f}_A)_m+(\mathbf{f}_P)_m-(\mathbf{f}_P)_n\cdot l_{\text{step}}}{(\mathbf{f}_A)_n+(\mathbf{f}_P)_n}$) with respect to the ankle of the active foot. Notice that the signs of the ZMP as well as the components used in its expression follow the definitions of coordinate axes in Fig. 3. Furthermore, in SSP, $\mathbf{f}_P = 0$, so the expression for ZMP location is reduced to $(\mathbf{f}_A)_m/(\mathbf{f}_A)_n$.

4. An Optimization Procedure for Determining Optimal Joint Trajectories and Spring Constants

In order to minimize the control energy in one walking cycle, the following performance index

$$J = \int_{t_1}^{t_5} \|\boldsymbol{\tau}_a(t)\|^2 \mathrm{d}t \ . \qquad (15)$$

is defined. The biped investigated in this paper is actuated by DC motors. In a DC motor, torque is proportional to current and the electrical power, which is consumed by the resistive effect of the motor coil, is proportional to the square of the current. Therefore, this index is proportional to the electrical energy consumed by the biped.

By (8), the performance index indeed is dictated by $\boldsymbol{\theta}_a(t)$ and $\mathbf{K}$. The constraints for minimizing the performance index can also be expressed in terms of $\boldsymbol{\theta}_a(t)$ and $\mathbf{K}$. In this section, an optimization procedure is proposed to determine optimal $\boldsymbol{\theta}_a(t)$ and $\mathbf{K}$ to minimize such a performance index. Because the biped experiences drastic dynamic change at postures 1, 3, 4 and 5 in the optimization, $\boldsymbol{\theta}_a(t)$ is assumed to be a concatenation of three vectorial, polynomial trajectories $\boldsymbol{\theta}_{a_\text{SSP}}(t)$, $\boldsymbol{\theta}_{a_\text{DSP1}}(t)$ and $\boldsymbol{\theta}_{a_\text{DSP2}}(t)$ respectively defined in $[t_1, t_3]$, $[t_3, t_4]$ and $[t_4, t_5]$ and parameterized as follows:

$$\begin{aligned}
\boldsymbol{\theta}_{a_\text{SSP}}(t) &= \mathbf{A}_{\text{SSP}}\mathbf{h}(t), && \text{for } t \in [t_1, t_3] \\
\boldsymbol{\theta}_{a_\text{DSP1}}(t) &= \mathbf{A}_{\text{DSP1}}\mathbf{h}(t), && \text{for } t \in [t_3, t_4] \\
\boldsymbol{\theta}_{a_\text{DSP2}}(t) &= \mathbf{A}_{\text{DSP2}}\mathbf{h}(t), && \text{for } t \in [t_4, t_5] \,,
\end{aligned} \qquad (16)$$

where $\mathbf{h}(t) = [1 \ \ t t^2 \cdots t^m]^T$ with m being the order of polynomials, and $\mathbf{A}_{(\cdot)}$'s are matrices of suitable dimensions and contain parameters of the polynomial trajectories for the joints in the active leg. The optimization problem can now be posed as

$$\begin{aligned}
\min_{A_{\text{SSP}}, A_{\text{DSP1}}, A_{\text{DSP2}}, K} \Bigg(& \int_{t_1}^{t_3} \|\boldsymbol{\Gamma}_{\tau_a}(\mathbf{A}_{\text{SSP}}\mathbf{h}(t), \mathbf{K})\|^2 \mathrm{d}t \\
& + \int_{t_3}^{t_4} \|\boldsymbol{\Gamma}_{\tau_a}(\mathbf{A}_{\text{DSP1}}\mathbf{h}(t), \mathbf{K})\|^2 \mathrm{d}t \\
& + \int_{t_4}^{t_5} \|\boldsymbol{\Gamma}_{\boldsymbol{\tau}_a}(\mathbf{A}_{\text{DSP2}}\mathbf{h}(t), \mathbf{K})\|^2 \mathrm{d}t \Bigg) ,
\end{aligned} \qquad (17)$$

subject to (10), (11), (12), (13), (14) and the ZMP stability constraint.

in which the constraints, although they are expressed in terms of $\boldsymbol{\theta}(t)$ $(= [\boldsymbol{\theta}_a(t) \ \boldsymbol{\theta}_u(t)]^T)$, $\mathbf{f}_A$ and $\mathbf{f}_p$, can be alternatively expressed in terms of $\boldsymbol{\theta}_a(t)$ and $\mathbf{K}$ by (5), (6), (7) and (9).

In the optimization problem, non-linear, dynamic operators appear not only in the performance index but also in the constraints. It is obvious that the problem is not analytically solvable but has to be solved by numerical procedures. For the purpose of numerically solving the problem, we discretize the interval $[t_1, t_5]$ into N equal-spaced time instants (with N sufficiently large and t_3, t_4 being two of the time instants) and approximate each of the integrals in (17) by a summation of $\|\boldsymbol{\Gamma}_{\boldsymbol{\tau}_a}(\cdot, \cdot)\|^2$ evaluated at all the time instants at the respective intervals. Furthermore, the continuous inequalities in (13), (14) and the ZMP stability constraint are also evaluated at all the time instants at the respective interval(s) to construct a set of discretized inequalities.

The discrete form of the problem is in a standard format for non-linear, constrained optimization in MATLAB® Optimization Toolbox, so the function *fmincon* in this package is used to solve the problem numerically. The *fmincon* is basically a sequential quadratic programming (SQP) method. It first converts the problem into a set of Kuhn-Tucker (KT) equations, whose solution forms the necessary condition for optimality for the constrained optimization problem. Then the KT equations are solved numerically using the iterative quadratic programming procedure. At each iteration, the numerical values of the gradient and the Hessian of the performance index and the gradient of the constraint functions are analyzed in order to determine the direction of parameter search and the appropriate step size. Although the analytic forms of the performance index and constraint functions are not explicitly given, their functional values are computed numerically at each step and the gradients and the Hessian are then obtained using a quasi-Newton method. The details of the iterative procedure can be found in Gill, Murray, and Wright[13] and Coleman and Zhang.[14]

When the *fmincon* function is used to solve the values for the optimal $\mathbf{A}_{(\cdot)}$ and $\mathbf{K}$, it is found that due to the vast numbers of parameters and constraints involved, convergence of the numerical iteration is not easy to achieve. In order to obtain a convergent solution for the relevant parameters but still maintain their optimality to a certain degree, four modifications are made to the optimization problem. First,

https://doi.org/10.1017/S0263574708005225 Published online by Cambridge University Press

it is assumed that the bounds for each of the diagonal components of **K** are given. Rather than finding **K** directly using the *fmincon* function, the solution space of **K** is divided into a grid and the optimization problem is solved repeatedly for each grid point in a brute force manner. The solution that results in the lowest performance index is adopted as the optimal one. With this modification, the number of free parameters in each optimization is reduced and convergence is easier to achieve. The computation time associated with such a brute force search is also not over-demanding because from the symmetric design of the two legs, the dimension of the solution space for **K** is low (3 for the sagittal dynamics, and 2 for the frontal dynamics).

Second, the constraint associated with ZMP stability is relaxed when solving the optimization problem. Such a stability condition is examined after an optimal solution is reached. If ZMP stability does not hold, depending on which phase(s) it is violated, the respective time duration(s) ($t_1 - t_3$ for SSP, and $t_3 - t_5$ for DSP) is (are) lengthened. By lengthening the time duration(s), the speed, consequently the dynamic effect, of the biped is reduced and it is easier to make the ZMP stable. Notice that the lengthening of time duration(s) can be done in an iterative manner so that the average walking speed is maintained at an acceptable level.

Third, instead of solving the values for all the three $\mathbf{A}_{(\cdot)}$ matrices simultaneously, the three integrals in (17) are minimized separately in a sequential manner. The sequential optimization is conducted in the way that $\boldsymbol{\theta}_{a_SSP}(t_3)$ ($= \mathbf{A}_{SSP}\mathbf{h}(t_3)$) and $\dot{\boldsymbol{\theta}}_{a_SSP}(t_3)$ ($= \mathbf{A}_{SSP}\dot{\mathbf{h}}(t_3)$) obtained from minimizing the first integral are substituted as initial conditions for the optimization of the second integral, and $\boldsymbol{\theta}_{a_DSP1}(t_4)$ ($= \mathbf{A}_{DSP1}\mathbf{h}(t_4)$) and $\dot{\boldsymbol{\theta}}_{a_DSP1}(t_4)$ ($= \mathbf{A}_{DSP1}\dot{\mathbf{h}}(t_4)$) obtained from minimizing the second integral are substituted as initial conditions for the optimization of the third integral. With such a modification, one has to deal with only one of the three $\mathbf{A}_{(\cdot)}$ matrices in each optimization, but the set of $\mathbf{A}_{(\cdot)}$ matrices resulted is considered to be only a sub-optimal solution.

Finally, in the simulation for computing the optimal $\mathbf{A}_{SSP}$ that minimizes the first integral in (17), it is found that numerical convergence still cannot be achieved. The failure in convergence is attributed to the strict constraints, particularly the foot-ground clearance constraint. To bypass the convergence issue, one observes from the kinematics of the biped that its step-size, which is relevant to the posture constraints, is mainly dictated by the hip joint motion. Based on this reasoning, the $\mathbf{A}_{SSP}$ matrix is decomposed as $\mathbf{A}_{SSP} = [\bar{\mathbf{A}}_{SSP}^T\ \mathbf{a}]^T$, in which the vector **a** contains parameters of the polynomial trajectories for the hip joint, and $\bar{\mathbf{A}}_{SSP}$ contains parameters for the rest of the joint(s) (ankle joint only for the frontal dynamics, and knee and ankle joints for the sagittal dynamics). Then the optimization problem is divided into two parts. The first part assumes **a** given $\bar{\mathbf{A}}_{SSP}$ and computes the optimal **a**, which satisfies only the posture constraint and the non-sliding constraint. The second part assumes a given **a** and computes the optimal $\bar{\mathbf{A}}_{SSP}$, that satisfies only the foot-ground clearance constraint and the non-sliding constraint. These two optimizations are cross-iterated until the 2-norm of the difference between the values of the two $\boldsymbol{\theta}_{a_SSP}(t)$ from the two optimizations converges to within a preset tolerance (say, 10^{-5}). The converged solution from the iterative optimization procedure is expected to minimize the control energy during the SSP and satisfy the relevant constraints to within the order of magnitude of the pre-set tolerance.

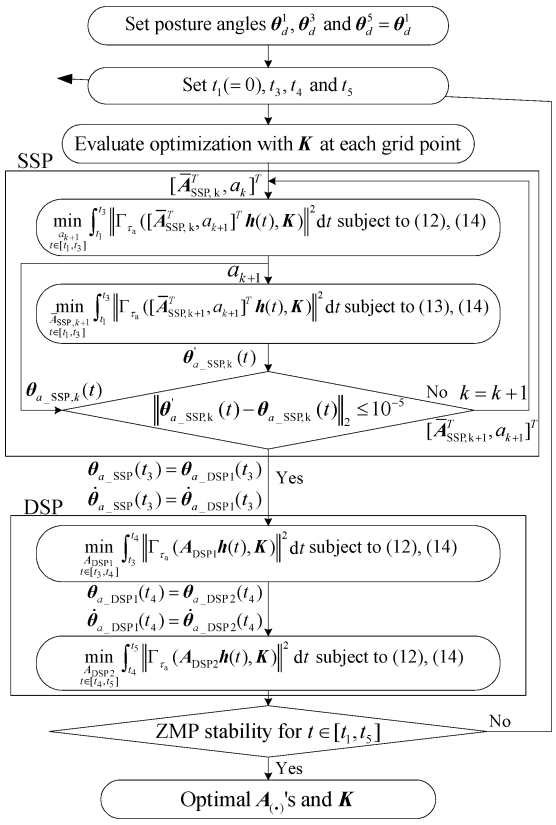


Fig. 4. The flow chart of optimization procedure.

The flow chart of the final optimization procedure that incorporates the four modifications is depicted in Fig. 4. In this flow chart, the parameters and initial conditions needed for initiating the optimization procedure are $\boldsymbol{\theta}_d^1$, $\boldsymbol{\theta}_d^3$, t_3, t_4, t_5, the range of each component in **K**, and finally the initial guesses for $\mathbf{A}_{SSP}$, $\mathbf{A}_{DSP1}$, $\mathbf{A}_{DSP2}$. Except for t_3, t_4 and t_5, the rest of the parameters and the initial guesses can be chosen systematically in the following manner: $\boldsymbol{\theta}_d^1$, $\boldsymbol{\theta}_d^3$ are chosen so that they make the bipedal mimic a gait similar to human walking with a consistent step size. The range of each component in **K**, which is used for the grid-point search of the optimal spring constant, is set to equal to the maximum among the appended spring constants ($k'_{i,*}$'s) computed later in (19) with $k_{i,*} = 0$. The initial guesses for $\mathbf{A}_{SSP}$, $\mathbf{A}_{DSP1}$, $\mathbf{A}_{DSP2}$ are respectively set to $[\boldsymbol{\theta}_d^1\ \mathbf{0} \cdots \mathbf{0}]$, $[\boldsymbol{\theta}_d^3\ \mathbf{0} \cdots \mathbf{0}]$, $[\boldsymbol{\theta}(t_4)\ \mathbf{0} \cdots \mathbf{0}]$, in which $\boldsymbol{\theta}(t_4)$ is obtained from minimizing $\int_{t_3}^{t_4} \|\boldsymbol{\Gamma}_{\tau_a}(\mathbf{A}_{DSP1}\mathbf{h}(t), \mathbf{K})\|^2 dt$. By doing so the procedure uses constant angles as the initial trajectories to solve for the sub-optimal solution. As for t_3, t_4, t_5, for simplicity only t_5 needs to be chosen and t_3, t_4 are respectively set as $t_5/3$ and $2t_5/3$; t_5 has to be chosen in an iterative manner for achieving not only an acceptable walking speed, but also a converging $\mathbf{A}_{SSP}$ and a stable ZMP trajectory.

https://doi.org/10.1017/S0263574708005225 Published online by Cambridge University Press

Table I. Kinematic parameters of the bipedal model.

	Shank ($i=1$)	Thigh ($i=2$)	Pelvis ($i=3$)	
Length l_i(m)	0.1	0.1	0.09	
Mass m_i (kg)	0.25	0.24	0.19	
Center of mass $r_{cx,i}$ (m)	0	0	0.045	
Center of mass $r_{cy,i}$ (m)	−0.01	−0.01	−0.01	
Center of mass $r_{cz,i}$ (m)	0.01	0.085	0.025	

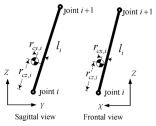


Table II. Assigned configurations at postures 1 and 3.

	$\theta_{1,p}$	$\theta_{2,p}$	$\theta_{3,p}$	$\theta_{1,r}$	$\theta_{3,r}$
Posture 1	$\frac{18.0}{180}\pi$	$\frac{33.1}{180}\pi$	$\frac{-20.0}{180}\pi$	$\frac{22.5}{180}\pi$	$\frac{22.5}{180}\pi$
Posture 3	$\frac{13.9}{180}\pi$	$\frac{30.8}{180}\pi$	$\frac{-0.65}{180}\pi$	$\frac{22.5}{180}\pi$	$\frac{22.5}{180}\pi$

Unit: radian.

5. Simulation Results

The optimization procedure is applied to the bipedal model with parameters listed in Table I. The assumed actuated joint angles at postures 1 and 3 are listed in Table II and the postures lead to $l_{\text{step}} = 8$ cm. It is also assumed that $t_1 = 0$ s, $t_3 = 0.5$ s, $t_4 = 1$ s, $t_5 = 1.5$ s, so the average speed is 2.67 cm/ s. The relaxed spring angles for the ankle, knee and hip are taken as the averages of the associated joint angles at postures 1 and 3. The viscous damping coefficient for each joint and the coefficient of static friction (μ_s) between the foot and the ground are respectively chosen† as 0.488 N· m· s/rad and 1.05.

In the optimization, the joint trajectories of the active leg are chosen as seventh-order polynomials. Using the flow chart in Fig. 4, the optimal values of $\mathbf{A}_{(\cdot)}$ and $\mathbf{K}$ are successfully computed. Notice that although the control energy is minimized in this case, it is under the assumption that all the springs obey linear constitutive relations. Apparently, if one relaxes this assumption or makes the springs non-linear, it is very likely that the control energy can be further reduced. Intuitively, the swing leg, when equipped with compliant springs, is easier to swing, but the support leg, when equipped with stiff joint springs, demands less control authority because the restoring torques from the springs are more significant to counteract the gravity. In order to accommodate the needs for swinging and supporting simultaneously, in addition to the original linear spring, we consider appending another spring to the joint so that one end of the spring is attached to one of the adjacent links, and the other end is free but is set at a designated angle. When the joint rotation is small, this appended spring is in an idle state. However, when the joint rotation exceeds the designated angle, the free end is compressed by the other link and the restoring torque is generated. Here the two-spring combination at each joint is referred to as the composite spring. The constitutive relationship for the composite spring at the ith joint can be written in a piecewise-linear manner:

$$\tau_i^k(\theta_{i,*}) = \begin{cases} k_{i,*}\cdot(\theta_{i,*} - \bar{\theta}_{i,*}) \text{ , if } \theta \le \bar{\theta}'_{i,*} \\ k_{i,*}\cdot(\theta_{i,*} - \bar{\theta}_{i,*}) + k'_{i,*}\cdot(\theta_{i,*} - \bar{\theta}'_{i,*}), \text{ else.} \end{cases} \tag{18}$$

in which τ_i^k is the composite spring torque, $k_{i,*}$ and $k'_{i,*}$ are respectively the constants of the original linear spring and the appended spring, $\bar{\theta}_{i,*}$ is the relaxed angle of $k_{i,*}$, $\bar{\theta}'_{i,*}$ is the activation angle (or the free-end angle) for $k'_{i,*}$, and $* = p$ (sagittal dynamics) or $* = r$ (frontal dynamics).

The torques of the composite springs replace $\mathbf{K}\cdot(\boldsymbol{\theta} - \bar{\boldsymbol{\theta}})$ in (2) and the optimization is reconducted using the modified dynamic equation. The optimization assumes that the values of $k'_{i,*}$ and $\bar{\theta}'_{i,*}$ are given and they are determined as follows. Because from Fig. 2 it is seen that the joints of either leg are bent mostly when it is the active leg at posture 3, in order for the the appended springs to support the biped's weight without hindering the swinging motion, the free-end angles (say, $\bar{\theta}'_{1,p}$, $\bar{\theta}'_{2,p}$ and $\bar{\theta}'_{3,p}$ for the sagittal dynamics) are set close to the corresponding joint angles at posture 3 (say, $\theta_{1,p}(t_3)$, $\theta_{2,p}(t_3)$ and $\theta_{3,p}(t_3)$). By doing so, the appended springs are only activated for the active leg near posture 3. As for determining the appropriate $k'_{i,*}$ value (say, $k'_{1,p}$, $k'_{2,p}$ and $k'_{3,p}$), in order for the composite springs to support the biped at posture 3, one simply sets

$$k'_{i,*} = \frac{g_{ai}(\boldsymbol{\theta}(t_3)) + k_{i,*}\cdot(\theta_{i,*}(t_3) - \bar{\theta}_{i,*})}{(\bar{\theta}'_{i,*} - \theta_{i,*}(t_3))}, \tag{19}$$

where $g_{ai}(\boldsymbol{\theta}(t_3))$ is the ith component of gravitational torque vector in (3) evaluated at $t = t_3$, $k_{i,*}$ is the linear spring constant obtained from the previous optimization (without $k'_{i,*}$), and the index i runs through all the joints in the active leg. Once the values for $k'_{i,*}$ and $\bar{\theta}'_{i,*}$ for one leg are determined, the corresponding values for the other leg can be obtained by symmetry.

Optimization with the assigned properties for the appended springs generates a new set of optimal $\boldsymbol{\theta}_a(t)$ and $\mathbf{K}$. The corresponding stick diagrams of the walking gait in the sagittal and frontal views are plotted in Fig. 5(a). To understand the mechanics of optimal semi-active walking, the trajectory of the center point of pelvis (CPP) is also plotted in Fig. 5(b). When the biped starts from SSP at posture 1, the CPP is located at 'a' or around the top of the front (left) foot. Distinct from other walking bipeds, the pelvis of the proposed biped is driven by the active (front) leg to move first forward and upward through 'b' and then backward and

† The two coefficients are obtained by performing identification experiments on the bipedal prototype. Particularly, the identification of coefficient of viscous friction is described in the next section.

https://doi.org/10.1017/S0263574708005225 Published online by Cambridge University Press

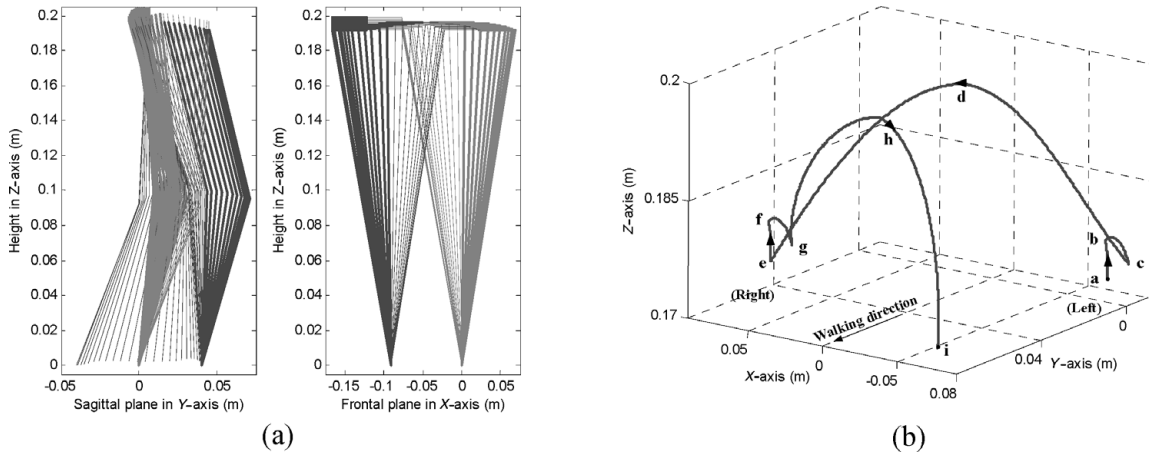


Fig. 5. (a) The consecutive stick figures of the walking gait in sagittal and frontal views. (b) The trajectories of the center point of pelvis of the biped.

downward to 'c'. By doing so, the passive foot, if the pelvis is maintained level, is first lifted off the ground to avoid foot scuffing and is then swung forward by the passive dynamics contributed by mechanical links and springs. Afterwards, by lowering the CPP, the passive foot lands on the ground and DSP starts. During DSP, the CPP is transmitted from the top of the rear (left) leg towards the top of the front (right) leg through '$c - d - e$' trajectory, and moreover, the actuation is transited at the middle point 'd'. When the transition finishes, the biped moves one step forward and returns to the initial posture except that the CPP is now shifted to the right and the two feet are exchanged.

The computed optimal linear springs' constants and the associated relaxed angles, as well as the assigned properties for the appended springs are listed in Table III. It should be noted that because the optimal linear spring in the ankle-roll direction is stiff enough to support the body weight at posture 3, the appended spring is not needed at this joint.

The foot-ground clearance and its vertical velocity of the passive foot during SSP are shown in Fig. 6. The passive leg can be swung without foot scuffing and the foot lands on the ground with zero vertical velocity. Therefore, there is no the energy loss due to foot-ground friction or impact.

In Fig. 7, the calculated ZMP trajectory and the stability polygons spanned by the supporting foot (feet) are shown. With the foot size of 6 cm × 4 cm, it is found that ZMP always stays inside the corresponding stable polygon during either SSP or DSP. Particularly, although ZMP during SSP moves back and forth, it is still within the stability polygon of the supporting foot. Consequently, the biped is dynamically stable.

To compare the energy efficiency of our semi-active biped to the fully powered biped, all springs are removed and all

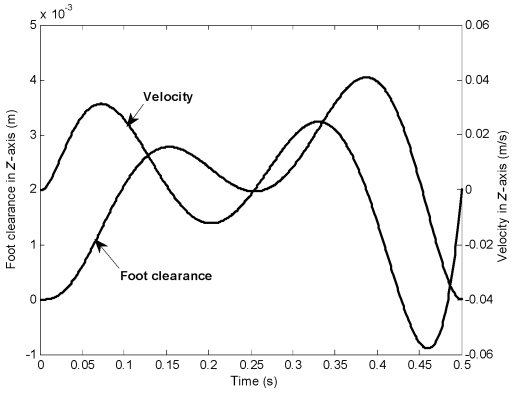


Fig. 6. The foot clearance and the vertical velocity of the passive foot during the SSP.

Table III. Springs' properties.

	Spring constant $k_{i,*}$(N · m/rad)	Relaxed angle $\overline{\theta}_{i,*}$(rad)	Spring constant $k'_{i,*}$(N · m/rad)	Relaxed angle $\overline{\theta}'_{i,*}$(rad)
Ankle-roll $(\cdot)_{1,r}$	0.66	$\frac{20}{180}\pi$	0.0	N/A
Ankle-pitch $(\cdot)_{1,p}$	0.075	$\frac{16.0}{180}\pi$	0.5	$\frac{18}{180}\pi$
Knee-pitch $(\cdot)_{2,p}$	0.25	$\frac{31.95}{180}\pi$	0.45	$\frac{27.5}{180}\pi$
Hip-roll $(\cdot)_{3,r}$	0.32	$\frac{20}{180}\pi$	0.87	$\frac{22.5}{180}\pi$
Hip-pitch $(\cdot)_{3,p}$	0.3	$-\frac{10.35}{180}\pi$	0.075	$\frac{-3.15}{180}\pi$

https://doi.org/10.1017/S0263574708005225 Published online by Cambridge University Press

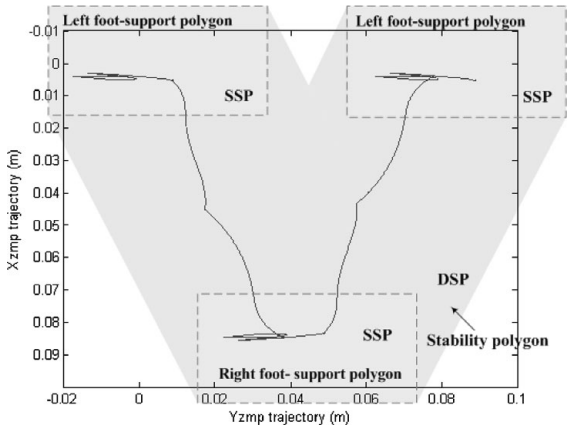


Fig. 7. The ZMP trajectory and the stability polygons.

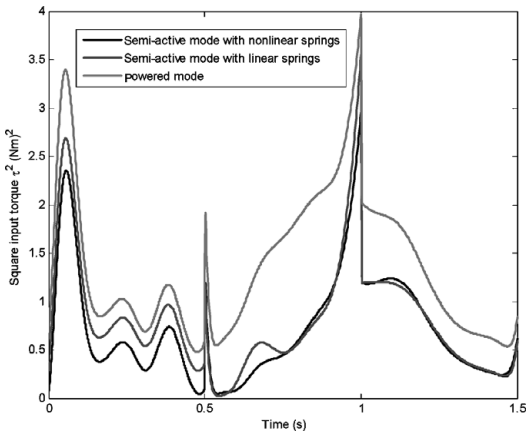


Fig. 8. The histories of square summation of input torques for the bipeds with linear/composite springs walking in the semi-active mode and powered mode.

the actuators are turned on to generate appropriate torques to make the biped follow the joint trajectories obtained from the optimization algorithm. The actuation torques are computed by directly substituting the joint trajectories into the dynamic equations. In Fig. 8, the histories of the square summation of all actuation torques respectively for the powered biped, the semi-active biped with linear springs, and the semi-active biped with composite springs are shown. It is found that in each walking cycle, the semi-active biped with linear springs consumes 60% less energy than the powered biped. With the composite springs, the semi-active biped can save 15% more energy. Notice that the extra savings in control energy occur

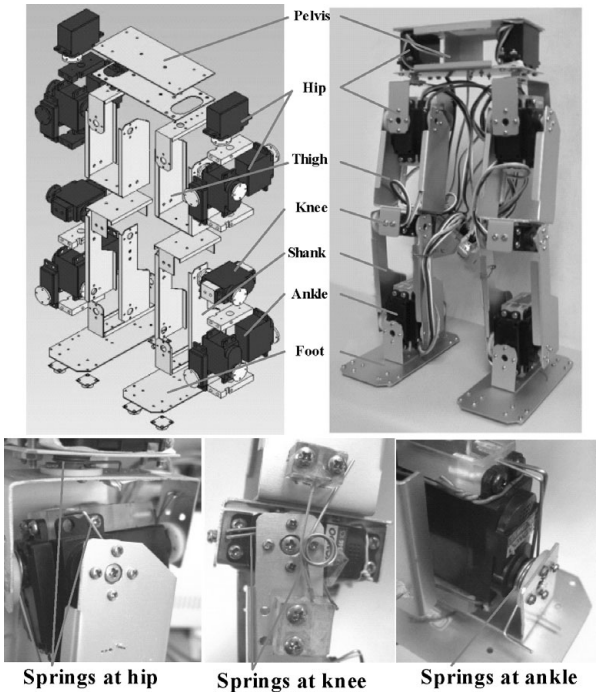


Fig. 9. The schematic drawing and the photo of the actual bipedal walker with parallel torsional coils attached at each joint.

mostly in SSP where the body weight is supported only by the active leg.

6. Hardware Implementation and Experimental Results

The 12-DOF model in Fig. 1 is converted into hardware. The schematic drawing and the photo of the actual biped are shown in Fig. 9. Torsional coils are attached to each joint to implement the composite spring design in the model. In the biped, the mechanical links are made of light aluminum alloy. DC servo motors with gear reduction are used as the actuators. The control block-diagram for the servo motor is depicted in Fig. 10. The block-diagram contains an inner loop for the current control and the outer loop for trajectory tracking. In the current control loop, the motor current is measured by a sensing resistor and is compared to the reference command. The error is then injected to a high-gain PI controller, which in turn computes the appropriate duty cycle for switching the H-bridge driver. The bandwidth of the current control loop is much higher than that of

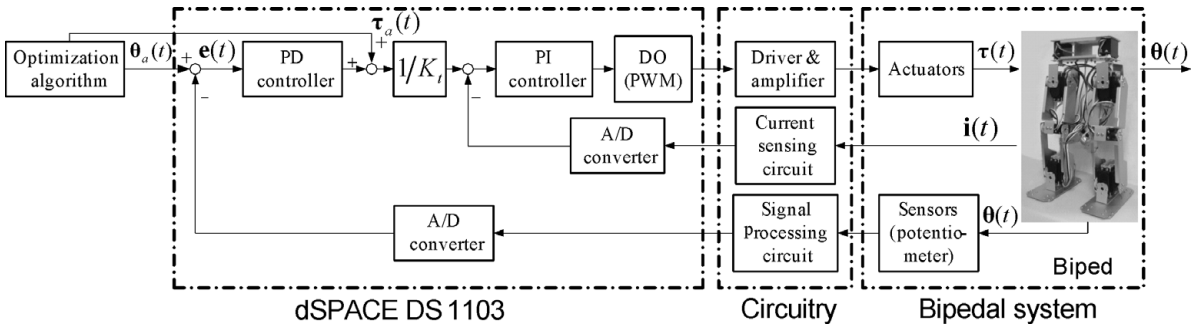
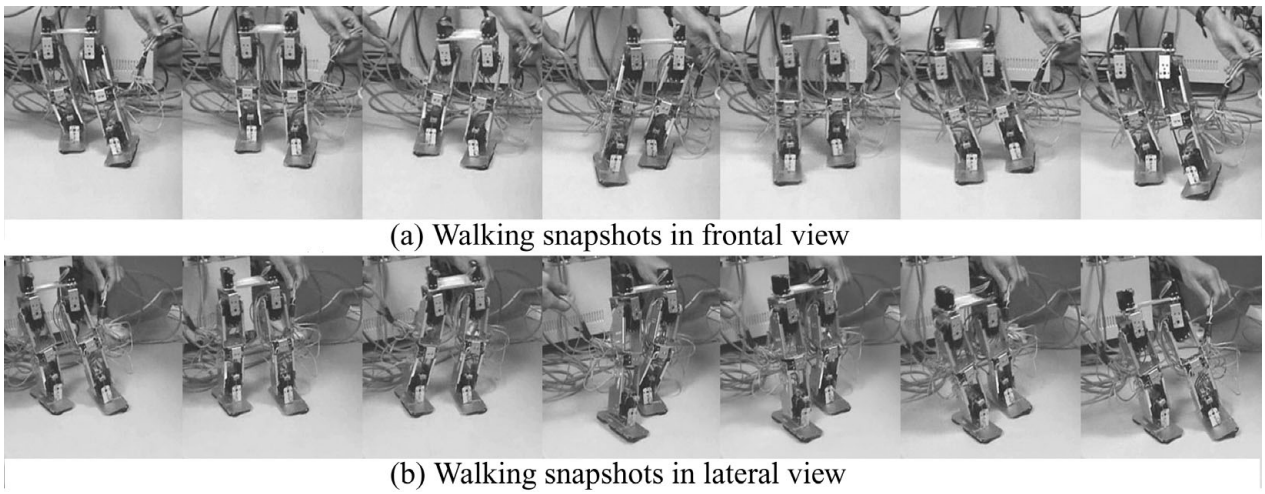


Fig. 10. The block diagram of the control algorithm.

https://doi.org/10.1017/S0263574708005225 Published online by Cambridge University Press



(a) Walking snapshots in frontal view

(b) Walking snapshots in lateral view

Fig. 11. The consecutive snapshots of the walking in front and lateral view. A more clear video demonstration can be found in http://ldsc.pme.nthu.edu.tw/files/Robot/SABW.wmv.

the mechanical dynamics, so the motors behave like torque motors. On the other hand, the outer loop incorporates PD feedback and feedforward compensation to control the motor torque to make the joint angle track a reference trajectory ($\boldsymbol{\theta}_a(t)$). Both $\boldsymbol{\theta}_a(t)$ and the feedforward torque ($\tau_a(t)$) are generated by the optimization procedure. The control system is carried out on a real-time digital signal processor (dSPACE^{TM} DS1103).

Empirically, it is found that static friction in the gear set is small and the motor is back-drivable when the current is off. Although the static friction is negligible, the viscous friction is not. The coefficient of viscous friction of the gear set (thus the joint) is experimentally identified by injecting a constant voltage to the motor to make it run at a constant speed. Then the motor circuit is open and the motor speed decays to zero. The decaying of the motor speed is a first-order response, so from the time constant and the equivalent inertia, one can estimate the coefficient of viscous friction.

6.1. Experiments for the semi-active walking motion

The springs' constitutive relations in Table III are used as the guidelines for choosing the torsional coils in the experimental biped. The $\boldsymbol{\theta}_a(t)$ adopted in the experiments follows similar trajectories as obtained from optimization with a particularly modification on the trajectory of the actuated ankle-roll joint during SSP. The modification is to account for the fact that while the shape of the foot is neglected in single-support phase of the simulation model, the small foot clearance ($\approx$4 mm) that resulted may render the swing foot of the experimental biped (whose foot size is not negligible) scuff the ground. One way to solve this problem is adding more roll rotation to the ankle in the active leg. By doing this way, the swing leg can be made to rotate away from the ground and scuffing does not occur. By a simple geometric calculation, a small roll rotation (about 3.9°) is added to the ankle of the active leg during SSP.

It should be noted that from the simulation point of view, the most intuitive way to avoid foot scuffing is replacing the foot-clearance constraint in (13) by $z_{\text{clearance}}(\theta(t)) \geq d(t)$, where $d(t) \geq 0$ is an appropriate lower bound of the swing foot trajectory for assuring sufficient foot clearance. However, such a replacement does not lead to a convergent solution in the optimization of the sagittal plane dynamics unless $\max_t d(t)$ is small enough ($\lessapprox$4 mm). This is due to the nature of semi-active walking that the swing foot is raised indirectly through actuating only the ankle, knee and hip-pitch joints of the active leg, so the foot height is very restricted. Although one can consider the coupling of sagittal and frontal dynamics so that the trajectories of the ankle-roll and/or hip-roll joints in the active leg can be incorporated in the optimization scheme to further raise the swing foot clearance, the coupling dynamics results in a 16th-order system that the convergence of numerical solution is even more difficult to achieve. Based on the above reasons, we resort to experimental tuning of the ankle-roll trajectory in the active leg to raise the swing foot clearance.

Fig. 11 shows the consecutive snapshots of the biped during one walking cycle with 1.5 s per step and a step length of about 8 cm. The video demonstration of the experiment can be found in http://ldsc.pme.nthu.edu.tw/files/Robot/SABW.wmv.[†] In the experiment, instead of switching the control authority instantly in middle of DSP as in simulation, the control gains of the active (passive) leg are changed smoothly from 100% (0%) to 0%(100%) within 1.5% of a walking cycle. By doing so, the jerky motion caused by instantaneous control authority transfer can be avoided.

6.2. Experimental power analysis

In Fig. 12, the histories of total electrical and absolute value of mechanical powers consumed in two walking cycle are recorded.[‡] For the purpose of comparing the energy

[†] A second prototype with on-board microprocessor, batteries and interfacing circuitry is also constructed. The prototype is operated without umbilical cords, but its motion is less smooth because the on-board microcomputer has much less computing power than the digital signal processor. Its video demonstration can be found in http://ldsc.pme.nthu.edu.tw/files/Robot/SABW2.wmv.

[‡] In the biped, the potentiometers, the signal conditioning circuits and drivers for the DC motors are powered by a 5-voltage power supply. The electrical power, which corresponds to the power

https://doi.org/10.1017/S0263574708005225 Published online by Cambridge University Press

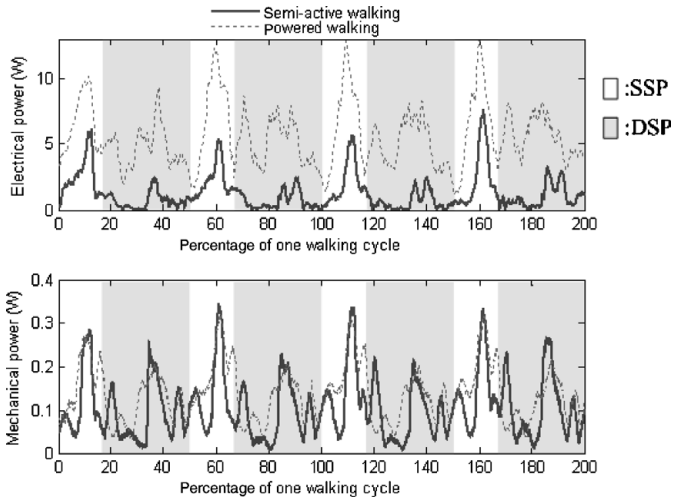


Fig. 12. The electrical and mechanical powers for the biped in the semi-active mode and the powered mode.

Table IV. The comparison of electrical energetic cost for the semi-active biped and other bipeds.

Walking object	C_{et}
Human	0.2
Our biped	1.81
T.U. Delft's Denise	5.3
MIT's Spring Flamingo	2.8
Honda's Asimo	3.2
Cornell's powered biped	0.2

efficiency of semi-active walking to powered walking, the torsional coils are removed and the biped walks in the powered mode. Although by the lower half of Fig. 12, the total mechanical powers of the two modes of walking are about the same, calculation on the upper half of the figure indicates that the powered walking mode consumes about five times the average electrical power of the semi-active mode. Such a phenomenon matches the previous argument on the use of springs to recover the negative work. In powered walking, some motors perform a significant amount of negative mechanical work. The negative electrical work associated with the negative mechanical work is not recoverable, so the total electrical power consumption is increased.

Here we also compare the energy efficiency of our biped with humans and other bipeds. To do so, a dimensionless energetic cost of transport C_{et} = (electrical energy)/(weight × traveled distance) is defined. This cost allows one to make fair comparison on the electrical energy efficiency regardless of the weights and the speeds of the bipeds. Table IV lists the C_{et} values for the human being, our biped and other bipeds.[15] Among the bipeds compared, Honda Asimo and MIT's SpringFlamingo both have actuators at all joints except that Spring Flamingo only performs 2-D walking and requires a tethering pole for maintaining stability in the lateral, roll and yaw directions. On the other hand, in T.U. Delft's Denise and Cornell's powered bipeds, only selected joints are equipped with actuators and the rest joints are passive. According to this table, although our biped is about an order of magnitude less efficient than the human walking, it is more efficient than the bipeds except Cornell's. Particularly, it is 43% more efficient than Honda Asimo, which uses electrical motors with high conversion efficiency (electrical energy to mechanical work) to perform powered walking. Clearly, it is the semi-active nature of our biped that allows it to outperform Asimo in the energy efficiency aspect. It should be noted that although Cornell's powered biped achieves the same walking efficiency as the human being, it has curved feet and only has two actuators (at the ankle) thus it could suffer stability problems.[15] Furthermore, it also cannot perform as dexterous motions as our biped, which is equipped with 12 actuators.

6.3. Further discussion on the swing-foot clearance

In the simulation of the optimal gait produced by the numerical procedure, the swing leg leaves the ground. Fig. 6 indicates that the swing-foot clearance, although small, always stays positive during swinging. It is not surprising to see the optimization procedure generating positive but small-foot clearance for the swing leg. This is because that to simultaneously minimize the input energy and avoid friction and impact, during the swing phase, the passive leg should avoid not only contacting the ground but also being lifted too high.

The optimization/simulation ideally assumes that the size of the swing foot is negligible but the actual biped does not obey such an assumption. In the ideal case the highest foot clearance for the swing leg is only 4 mm. Such a small foot clearance is not sufficient to make the sizable swing foot completely off the ground even if a small ankle-roll rotation is added. This is why the experimental video shows that the swing leg never leaves the ground. Although the swing leg never leaves the ground, the proposed mode of locomotion is not 'shuffling'. When a person walks by shuffling, he or she has to actuate the swing leg to make it move forward. Because the swing leg is actuated and never leaves the ground in this case, the normal force, consequently the friction force, is large and the energy consumption will be excessive. However, in the biped walking in the semi-active manner, the swing leg is unactuated. Furthermore, in Fig. 13, where the history of the normal force between the foot and the ground for one leg measured experimentally[†] is plotted, it can be found that the normal force during the swing phase (Phase D) is small. In fact, in about half of the swing phase, the normal force is nearly zero. Therefore the swing leg barely touches the ground and the biped does not walk in a shuffling manner. A similar semi-active gait can be observed in human walking.

consumed by the power supply, is measured by a wattmeter. On the other hand, the mechanical power is obtained by multiplying together the measured joint velocity and motor torque.

[†] When performing the experiment, the biped walks on two force plates that are aligned respectively with the left and right legs. The normal force history is recorded from the measurements of one of the force plates.

https://doi.org/10.1017/S0263574708005225 Published online by Cambridge University Press

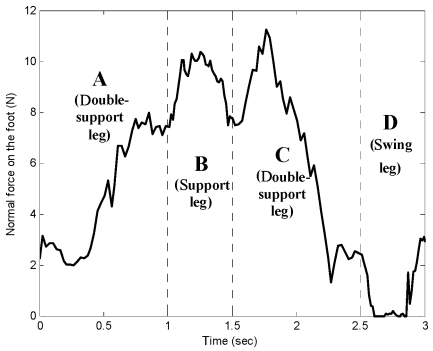


Fig. 13. The history of the normal force between the foot and ground for one leg measured in one walking cycle.

Imagine that a person is exhausted but still wants to walk forward. He/she tends to use least the muscles by relaxing the swing leg. He/she will use the total body motion to induce the movement of the swing leg. Moreover, in order to save the energy, he/she will not lift up the swing leg but will make it just barely touch the ground with minimum normal force.

The purpose of this paper is not to develop a biped that can outperform all other bipeds in every aspect. In fact, with only half of the joints actuated, the proposed biped certainly cannot achieve comparable walking performance as fully actuated bipeds. The message to be conveyed here is that when a biped is equipped with appropriate joint springs, there exists a semi-active gait that walking on level ground can be accomplished in an energy-efficient manner. Following the proposed optimization procedure, the optimal joint trajectories for such a gait and the corresponding joint springs can be systematically determined. The authors believe that a biped, like the human being, should adopt different modes of locomotion for different motion purposes and/or ground conditions. For instance, when the purpose is to walk on level ground with least energy consumption, then the biped should perform the proposed semi-active gait. If walking uphill or across obstacles is desired, then the biped should adopt power walking for generating dexterous motion such as lifting the swing leg off the ground.

7. Conclusions

In this paper, a biped that combines the merits of both powered and passive bipeds is proposed. The biped walks in the semi-active manner because during the walking cycle, only half of the motors are actuated. In order to fully exploit the semi-activeness for energy saving, the trajectories for the actuated joints and joints' spring constants are computed by an optimization procedure. The feasibility of the proposed biped, including the system design and the control performance, is verified by hardware implementation. Experiments indicate that the biped walking in the semi-active manner is indeed more energy-efficient than several state-of-the-art bipeds. It should be noted that in this research, the energy-efficient feature due to the semi-activeness is only demonstrated on a biped under quasi-static walking in which the ZMP always remains strictly within the interior of the support polygon. However, the concept of the semi-active walking is also potentially useful for dynamic walking in which the ZMP is on the boundary of the support polygon for at least part of the walking cycle and yet the biped does not overturn. In this case, by turning off part of the actuators in the swing leg, passive dynamics can be better exploited for power-saving purposes and fast, natural-looking motions as human walking can be resulted. Therefore, on-going research is devoted to developing the semi-active control strategy for bipeds that perform dynamic walking.

Acknowledgment

The authors gratefully acknowledge the support provided by National Science Council in Taiwan.

References

1. A. Takanishi, L. Hun-ok, M. Tsuda and I. Kato, 'Realization of dynamic biped walking stabilized by trunk motion on a sagittally uneven surface,' *Proceedings of the IEEE International Workshop on Intelligent Robots and Systems* (1990) pp. 323–330.
2. K. Hirai, M. Hirose, Y. Haikawa and T. Takenaka, 'The development of Honda humanoid robot,' *Proceedings of the IEEE International Conference on Robotics and Automation*, Leuven, Belgium (1998) pp. 1321–1326.
3. T. McGeer, 'Passive dynamic walking,' *Int. J. Robt. Res.* 9(2):62–82 (1990).
4. S.H. Collins, M. Wisse and A. Ruina, 'A three-dimensional passive dynamic walking robot with two legs and knees,' *Int. J. Robt. Res.* 20(7), 607–615 (2001).
5. S.H. Collins, A. Ruina, R. Tedrake and M. Wisse, 'Efficient bipedal robots based on passive-dynamic walkers,' *Science* 307(5712):1082–1085 (2005).
6. G. Bessonnet, P. Seguin and P. Sardain, 'A parametric optimization approach to walking pattern synthesis,' *Int. J. Robt. Res.* 24(7):523–536 (2005).
7. V. Sangwan and S.K. Agrawal, 'Leg-like motion with an under-actuated two DOF linkage using differential flatness,' *Proceedings of the 2006 American Control Conference*, Minneapolis, Minnesota, USA (2006) pp. 1790–1795.
8. K. Ono and R.Q. Liu, 'Optimal biped walking locomotion solved by trajectory planning method,' *ASME J. Dyn. Syst. Meas. Control* 124(4):554–565 (2002).
9. K. Ono, T. Furuichi and R. Takahashi, 'Self-excited walking of a biped mechanism with feet,' *Int. J. Robt. Res.* 23(1):55–68 (2004).
10. E. R. Westervelt, G. Buche, and J. W. Grizzle, 'Experimental validation of a framework for the design of controllers that induce stable walking in planar bipeds,' *Int. J. Robt. Res.* 24(6):55–68 (2004).
11. E. R. Westervelt, J. W. Grizzle, C. Chevallereau, J. H. Choi, and B. Morris, *Feedback Control of Dynamic Bipedal Robot Locomotion* (CRC Press, 2007, New York.)
12. A. Goswami, 'Postural stability of biped robots and the foot-rotation indicator (FRI) point,' *Int. J. Robt. Res.* 18(6):523–533 (1999).
13. T. F. Coleman and Yin. Zhang, Optimization Toolbox for use with MATLAB® (Version 2006b) (The MathWorks, Inc., 2006).
14. P.-E. Gill, W. Murray and M.-H. Wright, Practical Optimization, (Academic Press, New York, 1981).
15. S.H. Collins and A. Ruina, 'A bipedal walking robot with efficient and human-like gait,' *Proceedings of the IEEE International Conference on Robotics and Automation*, Barcelona, Spain (2005) pp. 1983–1988.

https://doi.org/10.1017/S0263574708005225 Published online by Cambridge University Press